Characterizing the influence of atmospheric river orientation and intensity on precipitation distributions over North Coastal California

Chad W. Hecht[1] (iD) **and Jason M. Cordeira[2]** (iD)

[1]Center for Western Weather and Water Extremes, Scripps Institution of Oceanography, University of California, San Diego, La Jolla, California, USA, [2]Department of Atmospheric Science and Chemistry, Plymouth State University, Plymouth, New Hampshire, USA

Abstract Atmospheric rivers (ARs) are long (>2000 km) and narrow (500–1000 km) corridors of enhanced vertically integrated water vapor and enhanced integrated water vapor transport (IVT) that are responsible for a majority of global poleward moisture transport and can result in extreme orographic precipitation. Observational evidence suggests that ARs within different synoptic-scale flow regimes may contain different water vapor source regions, orientations, and intensities and may result in different precipitation distributions. This study uses *k*-means clustering to objectively identify different orientations and intensities of ARs that make landfall over the California Russian River watershed. The ARs with different orientations and intensities occur within different synoptic-scale flow patterns in association with variability in IVT direction and quasi-geostrophic forcing for ascent and lead to different precipitation distributions over the Russian River watershed. These differences suggest that both mesoscale upslope moisture flux and synoptic-scale forcing for ascent are important factors in modulating precipitation distributions during landfalling ARs.

1. Introduction

A majority of the annual precipitation (30–50%) and extreme precipitation events in California and locations along the U.S. West Coast are attributed to the presence of atmospheric water vapor flux from lower latitudes along enhanced regions of integrated water vapor (IWV) and IWV transport (IVT) in long (>2000 km) and narrow (500–1000 km) corridors known as atmospheric rivers (ARs) [e.g., *Zhu and Newell*, 1998; *Ralph et al.*, 2004, 2006; *Ralph and Dettinger*, 2012]. *Zhu and Newell* [1998] discovered that ARs are responsible for >90% of meridional moisture transport while covering a small fraction of the globe (<10%). Landfalling ARs along the California coast are commonly associated with water vapor flux in a moist-neutral environment that can result in orographic precipitation along the Coast Ranges and Sierra Nevada [*Neiman et al.*, 2008]. Several factors such as the IVT direction, intensity, and duration along these landfalling ARs and the synoptic-scale dynamics of their parent winter storms (i.e., frontogenetic/frontolytic circulations, quasi-geostrophic forcing, and upper tropospheric jet circulations as discussed in *Cordeira et al.* [2013]) may combine to produce differing precipitation distributions and hydrological impacts. The purpose of this paper is to examine the different IVT directions and magnitudes of landfalling ARs over North Coastal California and to illustrate associated variability in the synoptic-scale dynamics and resulting local and regional precipitation distributions.

2. Background and Motivation

ARs with different IVT directions are known to produce different hydrological impacts across different watersheds. *Ralph et al.* [2003] highlighted the importance of ARs with different IVT directions to extreme precipitation by identifying how variations of ±10° in wind direction can modulate the location of orographically enhanced floods. For example, the IVT direction in a landfalling AR played a crucial role in generating record flooding in the Pescadero Creek watershed while creating only moderate flooding in the adjacent watershed near Santa Cruz, California. In a similar study, *Neiman et al.* [2011] demonstrate that ARs with similar IVT magnitudes, but different IVT directions produced floods in different watersheds depending on the aspect of the watershed topography in relation to AR orientation over western Washington. Studies by *Neiman et al.* [2013] and *Hughes et al.* [2014] illustrate the importance of IVT direction along an AR in the production of extreme precipitation in Arizona during an event in 2010. The south-southwesterly IVT direction along an

AR on 21–22 January 2010 allowed for water vapor flux through an area of lower terrain on the Baja Peninsula of Mexico, resulting in enhanced inland upslope water vapor flux over the northwest-southeast oriented Mogollon Rim in Arizona. ARs with different intensities, often defined by the IVT magnitude, and duration are also known to produce increasingly greater precipitation totals and streamflow volume. *Ralph et al.* [2013] found that differences in storm total upslope water vapor flux explain 74% of the variance in storm total precipitation in North Coastal California, while longer-duration ARs are associated with an exponential increase in storm total streamflow volume.

The focus of this paper is on landfalling ARs over North Coastal California that may subsequently influence precipitation and hydrological extremes across the Russian River watershed (RRW). Flooding is one of the main hydrologic extremes that can result from landfalling ARs over the RRW. For example, all seven floods that occurred on the Russian River from 1997 to 2006 were associated with landfalling ARs [*Ralph et al.*, 2006]. While flooding is a negative and potentially costly result of landfalling ARs over the RRW, the precipitation from ARs is also an important contributor to the annual water supply and can act to mitigate drought [*Dettinger et al.*, 2011; *Dettinger*, 2013]. Lake Mendocino, on the East Fork of the Russian River behind the Coyote Dam, is an important reservoir that provides flood control, water supply, recreation, and streamflow regulation. Establishing a more robust understanding of the meteorological processes that lead to extreme precipitation over the RRW will assist in decision support services pertaining to both flood control and water supply operations on reservoirs like Lake Mendocino. Results from this study will contribute to the development and implementation of Forecast Informed Reservoir Operations, a proposed management strategy that uses data from watershed monitoring and modern weather and water forecasting to help water managers selectively retain or release water from reservoirs in a manner that reflects current and forecasted conditions [*Ralph et al.*, 2014].

3. Data Sources and Methodologies

The National Centers for Environmental Prediction (NCEP)-Climate Forecast System Reanalysis (CFSR) versions 1 [*Saha et al.*, 2010] and 2 [*Saha et al.*, 2014] data set is used to identify IVT direction and magnitude of landfalling ARs and synoptic-scale characteristics during an 11 year period between 1 January 2004 and 31 December 2014. The data were obtained from the National Oceanic and Atmospheric Administration (NOAA) National Operational Model Archive and Distribution System. The study initially sought to complement the 10 water year period investigated by *Young et al.* [2017]; however, the subsequent analysis includes results for the full 11 year period as seasonal variations are not considered in this study. The NCEP-CFSR data set is contained on a grid that spans vertically from 1000 hPa to 1 hPa on 37 isobaric levels, horizontally with a spectral resolution of t384 (~38 km) that is obtained on a 0.5° latitude by 0.5° longitude grid, and temporally every 6 h. AR orientation and intensity are approximated by the IVT vector direction and magnitude, respectively, which are calculated following the methodology of *Neiman et al.* [2008] as

$$\overrightarrow{IVT} = \frac{1}{g}\int_{1000\text{ hPa}}^{300\text{ hPa}} q\overrightarrow{V}\,dp, \tag{1}$$

where q is the specific humidity, g is acceleration due to gravity, and $\overrightarrow{V}$ is the total horizontal vector wind.

Landfalling ARs are identified based on area-averaged 24 h daily mean (ending at 1200 UTC) IVT magnitude ≥200 kg m^{-1} s^{-1} over a domain that spans from 37.3°N to 39.6°N and from 125°W to 122.3°W that is chosen to encompass the RRW in its upper right quadrant (Figure 1a). This methodology is similar to past studies that define ARs based on threshold values of IWV or IVT [e.g., *Ralph et al.*, 2004, 2006; *Neiman et al.*, 2008, 2011; *Lavers et al.*, 2012; *Rutz et al.*, 2014]. Common instantaneous IVT magnitude thresholds utilized by past studies are 250 kg m^{-1} s^{-1} and 500 kg m^{-1} s^{-1} [i.e., *Ralph et al.*, 2004, 2006; *Neiman et al.*, 2008]. *Lavers et al.* [2012] applied an instantaneous IVT magnitude threshold that represented the 85th percentile of IVT magnitudes calculated over a 30 year period in order to identify the most intense landfalling ARs. The area-averaged daily mean IVT magnitude threshold chosen in this study ≥200 kg m^{-1} s^{-1} corresponds to a comparable 84th percentile of domain-averaged daily IVT magnitude calculated over a 32 year period (1 January 1979 to 31 December 2010). Many past studies also apply a length and width criteria in order to identify ARs [e.g., *Ralph et al.*, 2004; *Lavers et al.*, 2011; *Dettinger et al.*, 2011; *Rutz et al.*, 2014]. Since this study utilized domain-averaged daily IVT and not instantaneous IVT, a length and width criteria were not applied. The corresponding 24 h precipitation during the daily mean period is obtained from the NCEP Stage IV multisensor
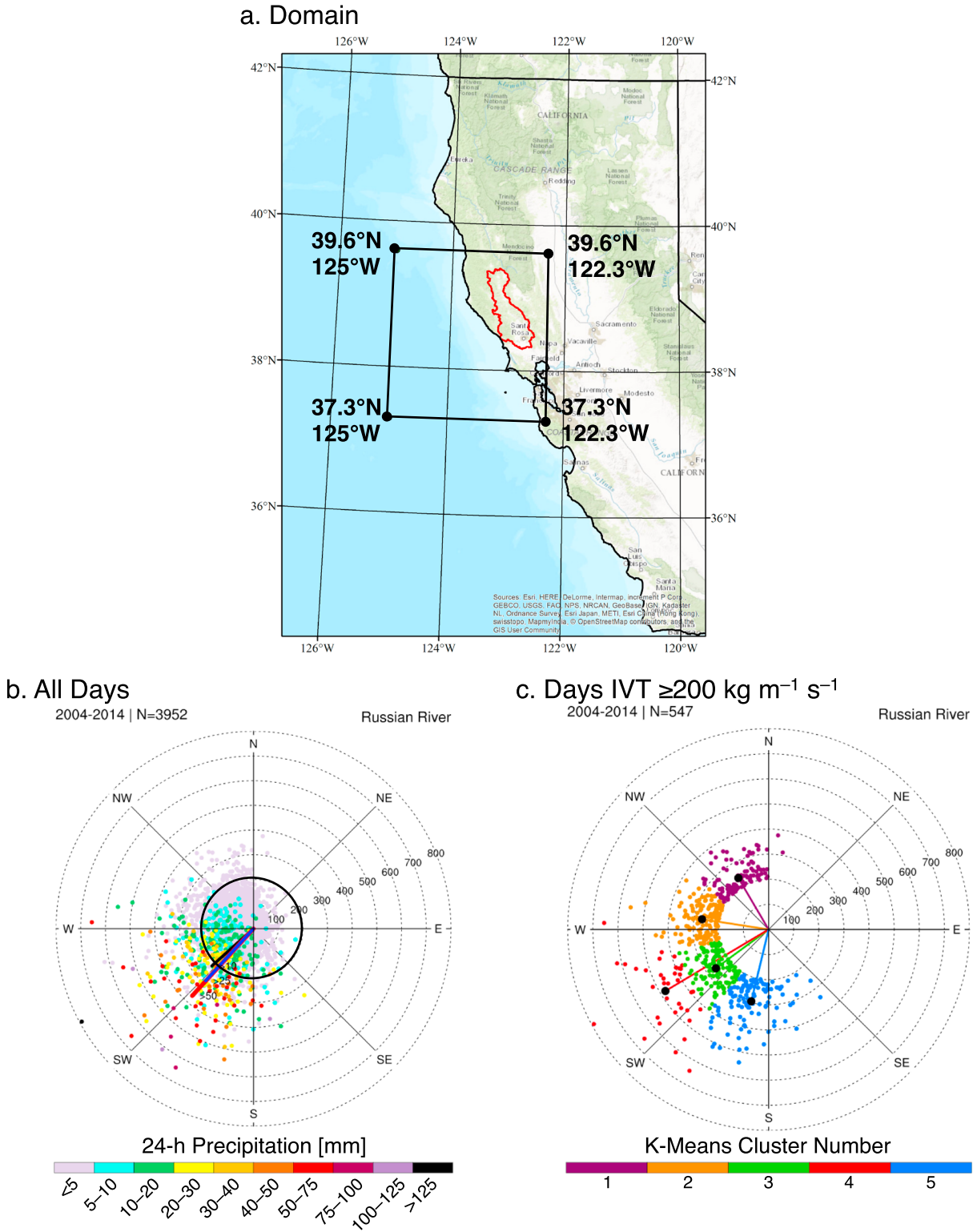
Figure 1. (a) A map of California and the Eastern North Pacific. The domain utilized to calculate area-averaged IVT (37.3°N to 39.6°N and from 125°W to 122.3°W) is outlined in black. The Russian River watershed is outlined in red. (b) Domain-averaged daily IVT direction (angular coordinate) and magnitude (kg m^{-1} s^{-1}; radial coordinate) for all days from 1 January 2004 to 31 December 2014 that data were available. Markers are color coded based on 24 h accumulated precipitation (mm). The colored lines illustrate the average IVT for days with precipitation >10 (black), >25 (blue), and >50 mm (red). The 200 kg m^{-1} s^{-1} threshold that was applied in this study is shown by the black circle. (c) As in Figure 1b except for days with daily average IVT ≥ 200 kg m^{-1} s^{-1} and color coded based on *k*-means cluster.

quantitative precipitation estimates on a 4 km × 4 km grid provided by the National Center for Atmospheric Research (NCAR) Earth Observing Laboratory [*Baldwin and Mitchell*, 1997]. The Stage IV precipitation data are valid only on the land portion of the map depicted in Figure 1a.

ARs with different orientations and intensities are objectively identified using a National Center for Atmospheric Research (NCAR) Command Language (NCL) [*The NCAR Command Language*, 2017] *k*-means clustering algorithm [*Hartigan and Wong*, 1979] that is applied to the *u* and *v* components of the area-averaged daily mean IVT vector. The NCL clustering algorithm allows the user to select the number of clusters defined and produced by the algorithm. Through trial and error, it was found that five clusters provided the best qualitative representation of landfalling ARs with different orientations and intensities over the RRW during the study period. Additional clusters decreased the sample size and subsequent composite members of each cluster, whereas fewer clusters increased the variance of daily IVT direction and magnitude within a given cluster.

Composite analyses are subsequently constructed using the days contained within each cluster to examine the synoptic-scale meteorological conditions associated with the clusters. The composite analyses are constructed at 0000 UTC (i.e., $t - 12$ h relative to the end of the 24 h period of precipitation). The synoptic-scale forcing associated with the different AR clusters is also illustrated via analysis of quasi-geostrophic (QG) forcing for ascent that is quantified using a methodology similar to *Cordeira et al.* [2013] by calculating the right-hand side of the Q-vector form of the QG omega equation evaluated at 700 hPa as in *Bluestein* [1992, equations (5.7.55) and (5.7.56)]. Regions of Q-vector convergence (divergence) are indicative of regions of QG forcing for ascent (descent) at 700 hPa. Q-vectors can also be used to diagnose lower tropospheric QG frontogenesis depending on the Q-vectors orientation relative to the 700 hPa potential temperature gradient [*Keyser et al.*, 1992]. The Q-vectors are calculated from smoothed composite average meteorological parameters and therefore represent regions in the composite that likely favor QG forcing for ascent or descent. Statistical significance of different cluster and composite populations is determined using an independent two-sided Student's *t* test.

4. Results

4.1. Cluster Analysis

The 11 year period from 2004 to 2014 contained 3952 days with available NCEP Stage IV 24 h accumulated precipitation and NCEP-CFSR area-averaged daily mean IVT data for the RRW (i.e., 98.4% data availability; Figure 1b). These data are plotted in rotated polar coordinates similar to a wind rose such that IVT magnitude is indicated by the radial coordinate, the IVT direction is indicated by the angular coordinate rotated such that a westerly water vapor flux is on the leftmost portion of the diagram, and the precipitation is indicated by the color shading of each marker. The polar coordinate diagram illustrates that larger precipitation totals tend to occur on days with larger IVT magnitudes from a southwest direction, as shown by *Ralph et al.* [2013]. The 11 year period contained 547 days with an area-averaged daily mean IVT magnitude ≥ 200 kg m^{-1} s^{-1} (Figure 1c). By employing the *k*-means clustering algorithm, these 547 days group into five different clusters related to their IVT magnitude and direction (i.e., their associated AR intensity and orientation): Cluster 1, northwesterly ($N = 115$); Cluster 2, westerly ($N = 143$); Cluster 3, southwesterly ($N = 137$); Cluster 4, strong southwesterly ($N = 36$); and Cluster 5, south-southwesterly ($N = 116$; Figure 1b). The clustering algorithm places each data point (i.e., a *u* and *v* component IVT pair) into the cluster whose centroid has the smallest Euclidian separation distance. While it may visually appear that some of the data points could "fit" into other clusters, each data point is objectively closest to its centroid. For brevity, the remainder of this paper focuses on the westerly cluster (Cluster 2) and the south-southwesterly cluster (Cluster 5). These clusters are chosen because they exhibited relatively similar centroid IVT magnitudes (268 kg m^{-1} s^{-1} and 294 kg m^{-1} s^{-1}, respectively), similar duration of instantaneous IVT magnitudes >250 kg m^{-1} s^{-1} (~18 h; not shown), quasi-orthogonal cluster centroid IVT directions (279° and 193°, respectively), and vastly different median area-averaged precipitation over the RRW (0.5 mm and 13.0 mm, respectively). For comparison, the cluster centroid IVT magnitude, IVT direction, and median area-averaged precipitation for the remaining clusters are (Cluster 1: northwesterly) 238 kg m^{-1} s^{-1}, 330°, 0 mm; (Cluster 3: southwesterly) 261 kg m^{-1} s^{-1}, 234°, 10.6 mm; and (Cluster 4: strong southwesterly) 479 kg m^{-1} s^{-1}, 239°, 40.2 mm, respectively.

4.2. Composite Analysis

Composite analyses of sea level pressure (SLP), IWV, and IVT reveal contrasting lower tropospheric synoptic-scale flow configurations associated with each cluster (Figures 2a and 2b). The westerly cluster occurs in association with a broad region of high pressure over the subtropical Northeast Pacific located to the south of a region of weak (~1004 hPa) low pressure over the Gulf of Alaska (Figure 2a), whereas the south-southwesterly cluster occurs in association with a bifurcated region of high pressure across the subtropical Northeast Pacific that straddles a more amplified and lower latitude region of low pressure near the U.S. West Coast (Figure 2b). Both clusters contain a corridor of enhanced IWV > 20 mm and IVT magnitude > 250 kg m^{-1} s^{-1} that is characteristic of a landfalling AR, albeit with different orientations and weak horizontal IWV gradients owing to composite smear. The westerly cluster illustrates an AR that extends west to east from ~145°W to the northern California and Oregon coastlines, whereas the south-southwesterly cluster illustrates an AR that extends southwest to northeast from ~135°W in the subtropics to the central California coastline.

The westerly cluster occurs on average in association with zonal flow at 250 hPa that contains a 55–60 m s^{-1} jet streak over the Northeast Pacific (Figure 2c), whereas the south-southwesterly cluster occurs on average in association with a negatively tilted trough and cyclonically curved jet streak at 250 hPa over the Northeast Pacific (Figure 2d). Each of these upper tropospheric synoptic-scale configurations has the potential to influence the evolution of landfalling ARs and associated precipitation. For example, the descent and concomitant lower tropospheric divergence linked to the descending branches of these thermally indirect ageostrophic circulations in the exit region of the upper tropospheric jets could result in water vapor flux divergence, decreasing IWV, and a weakening AR (e.g., as described by *Cordeira et al.* [2013]), and a decrease in subsequent orographic precipitation. The QG forcing for descent in the equatorward exit region of the westerly upper tropospheric jet streak may also lead to synoptic-scale subsidence over California and create an unfavorable environment for widespread precipitation or seeding of orographic precipitation [e.g., *Bergeron*, 1965; *Kingsmill et al.*, 2016]. Alternatively, the QG forcing for ascent associated with upper tropospheric divergence of the ageostrophic wind in the exit region of the cyclonically curved upper tropospheric jet streak [*Beebe and Bates*, 1955] combined with the divergence downstream of the negatively tilted trough, inferred through mass continuity, may create a favorable environment for widespread precipitation or seeding of orographic precipitation.

The QG forcing is summarized for the westerly cluster by a broad region of Q-vector convergence located over the Pacific Northwest Coast and a region of Q-vector divergence located over Southern California that favors a region of QG forcing for ascent north of the RRW and a region of QG forcing for descent south of the RRW (i.e., neutral forcing over the RRW; Figure 2e). The Q-vectors located over the terminus of the composite AR and North Coastal California are oriented toward regions of colder potential temperatures, indicative of lower tropospheric geostrophic frontolysis. A frontolytic circulation over the AR would favor IVT divergence within the terminus of the AR, resulting in a decrease in IWV and a weakening of the AR [*Cordeira et al.*, 2013]. The QG forcing is summarized for the south-southwesterly cluster by a broad region of Q-vector convergence located over North Coastal California that favors a region of QG forcing for ascent over the RRW (Figure 2f). These differences in locations of QG forcing for ascent contribute to differences in precipitation over North Coastal California and the RRW during landfalling ARs that occur in each cluster, such as revealed with the area-averaged precipitation results described earlier and in the following section.

4.3. Precipitation Analysis and Discussion

The precipitation distributions over North Coastal California and the RRW during landfalling ARs are illustrated via the 90th percentile 24 h accumulated precipitation values for each cluster population (Figure 3). The 90th percentile value is chosen as a measure of the "maximum case" (MC) precipitation, which is similar to probabilistic products produced from ensemble forecast guidance by the National Weather Service [*National Weather Service*, 2015]. The largest MC precipitation values (~100–110 mm) associated with the westerly cluster are confined to the Klamath Mountains and North Coast Ranges near the California-Oregon border where (1) the daily average IVT direction is more orthogonal to regional topography (Figure 3a) and (2) the middle troposphere is characterized by QG forcing for ascent (Figure 2e). The MC precipitation values over the RRW are less (~15–20 mm) than the surrounding areas, likely due to (1) a less orthogonal daily average IVT direction relative to the northwest to southeast oriented North Coast
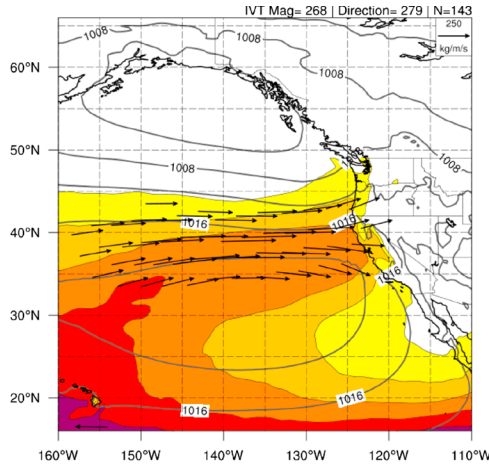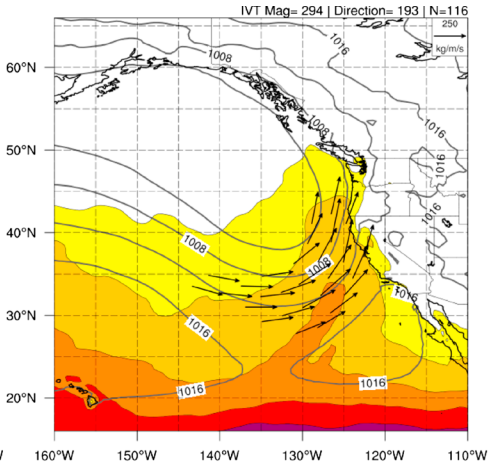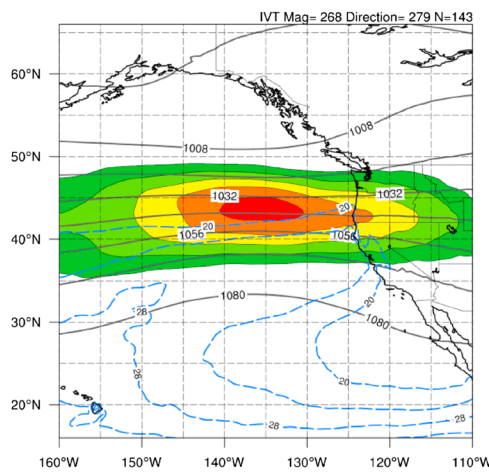
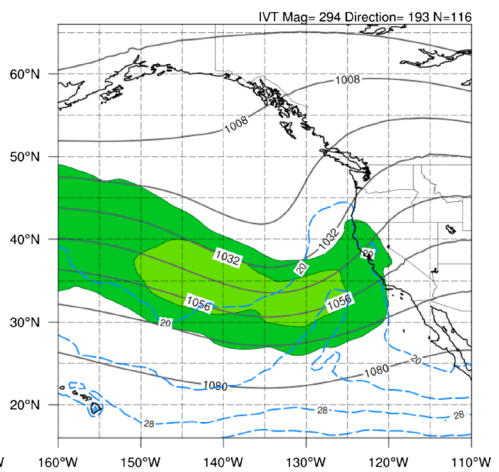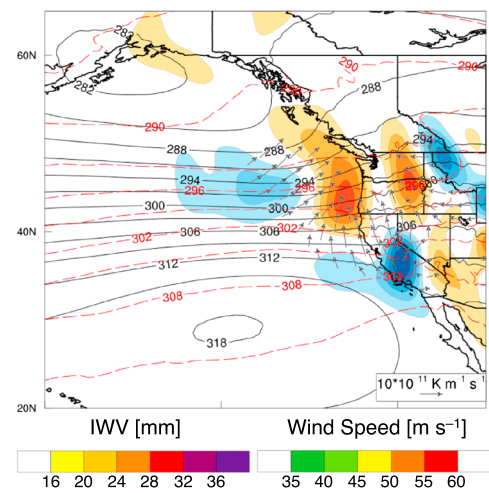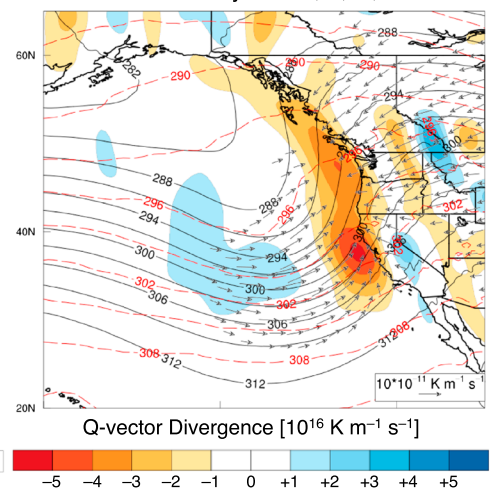**Figure 2.** (a, b) Composite mean IVT (kg m^{-1} s^{-1}; plotted according to the reference vector in the upper right), SLP (hPa; contoured), and IWV (mm; color coded according to scale); (c, d) composite mean 250 hPa geopotential height (dam; contoured), wind speed (m s^{-1}; color coded according to scale), and IWV (mm; dashed blue contour); and (e, f) composite mean 700 hPa geopotential height (dam; solid contours), Q-vectors (10^{11} K m^{-1} s^{-1}; plotted according to the reference vector in the bottom right), Q-vector divergence (10^{16} K m^{-1} s^{-1}; color coded according to scale), and potential temperature (K; dashed red contours) at $t - 12$ h during westerly (Figure 2a, 2c, and 2e) and south-southwesterly (Figure 2b, 2d, and 2f) ARs.

Figure 3. The 90th percentile of cluster population 24 h accumulated precipitation (mm; color coded according to scale) over Central California and composite mean 24 h average IVT (kg m^{-1} s^{-1}; plotted according to the reference vector in the upper right) for (a) westerly ARs and (b) south-southwesterly ARs. The Russian River Watershed is outlined in red. (c) The 30 m resolution digital elevation model (m; shaded according to scale) of the Russian River Watershed area (black outline) from the U.S. Department of Agriculture Natural Resources Conservation Service.

Figure 4. Box and whisker plots of Russian River Watershed (a) area average 24 h precipitation (mm), (b) domain average IVT (kg m^{-1} s^{-1}), (c) domain average lower tropospheric (1000–850 hPa) IVT (kg m^{-1} s^{-1}), (d) domain average Q-vector divergence (10^{16} K m^{-1} s^{-1}), and (e) domain average IWV (mm) for westerly (orange) and south-southwesterly (blue) ARs. The boxes represent the interquartile range of the data, and the whiskers represent upper and lower quartiles of the data. The horizontal line within the boxes is the median value. The colored dots represent outliers, and the asterisks represent extreme outliers. The box in the top left corner of each panel indicates the result of the independent samples *t* test with 95% confidence (white indicates significantly statistically similar means and black indicates significantly statistically different).

Ranges along the western periphery of the RRW and (2) neutral QG forcing for ascent. The largest MC precipitation values (~90–100 mm) associated with the south-southwesterly cluster are located over the Trinity Alps in North Coastal California, the RRW Coast Ranges, and in California's interior along the northern Sierra Nevada where (1) the daily average IVT direction is more orthogonal to regional topography (Figure 3b) and (2) the middle troposphere is characterized by QG forcing for ascent (Figure 2f). The local maximum in precipitation over the Trinity Alps and Mount Shasta is commonly observed during Sierra Barrier Jet events [*Ralph et al.*, 2016]. Future work should further investigate whether this feature is driven by the Sierra Barrier Jet and/or the inland penetration of IVT associated with the AR through the lower elevation San Francisco Bay gap and northward up the California Central Valley. The MC precipitation values over the RRW are comparable (~70–90 mm) to surrounding areas and 60 mm greater than the westerly cluster, likely due to (1) a more orthogonal daily average IVT direction relative to the northwest to southeast oriented North Coast Ranges along the western periphery of the RRW (Figure 3c) and the (2) QG forcing for ascent.

The median area-averaged precipitation over the RRW (Figure 4a) is significantly larger for the south-southwesterly cluster (13.0 mm) as compared to the westerly cluster (0.5 mm). This difference in RRW area-averaged precipitation is not likely explained by statistically similar cluster IVT magnitudes (i.e., AR intensity; Figure 4b) and IWV values (Figure 4e) but likely a combination of a more favorable southwesterly IVT direction (i.e., AR orientation) relative to the orientation of the local topography (Figure 3c) and favorable synoptic-scale forcing for ascent (Figure 2) illustrated by Q-vector convergence (Figure 4d). The difference may also be related to possible mesosynoptic-scale interactions related to seeding of orographic precipitation from synoptic-scale precipitation [e.g., *Bergeron*, 1965; *Kingsmill et al.*, 2016], consideration of local stability and the development of a coastal barrier jet [*Chao*, 1985], or the strength of the low-level jet stream [*Browning and Pardoe*, 1973]. While the former two processes are beyond the scope of this investigation on AR intensity and orientation, the latter may be quantified by the lower tropospheric IVT magnitude calculated for 1000–850 hPa (Figure 4c) as compared to 1000–300 hPa in equation (1). The lower tropospheric IVT magnitudes are on average statistically significantly larger for the south-southwesterly cluster (~115 kg m^{-1} s^{-1}) as compared to the westerly cluster (~75 kg m^{-1} s^{-1}; Figure 4c). This result supports findings from past studies that identify the importance of moisture transport in the lowest 1–1.5 km as a key ingredient in upslope moisture flux and orographic precipitation over the RRW [*Neiman et al.*, 2002; *Ralph et al.*, 2013].

5. Concluding Summary

This study used a *k*-means clustering algorithm and composite analysis in order to investigate synoptic-scale characteristics of landfalling ARs and precipitation over North Coastal California and the RRW. The composite analysis focused on two AR clusters associated with predominantly westerly and south-southwesterly IVT directions with comparable IVT magnitudes and different RRW area-averaged precipitation. These composite analyses illustrated that westerly ARs tend to be associated with less precipitation over the RRW due to less favorable synoptic-scale forcing for ascent related to neutral Q-vector divergence, a less favorable IVT direction as compared to the orientation of local topography, and lesser IVT magnitudes in the lowest 1–1.5 km of the atmosphere. Alternatively, south-southwesterly ARs tend to be associated with more precipitation over the RRW due to more favorable synoptic-scale forcing for ascent related to Q-vector convergence, a more favorable IVT direction as compared to the orientation of local topography, and larger IVT magnitudes in the lowest 1–1.5 km of the atmosphere. Specifically, the south-southwesterly oriented ARs allow for moisture flux over the lower elevations of the southern RRW (Figure 3c.), leading to orographic enhancement within the northern and eastern portions of the watershed. Penetration of IVT into the RRW during westerly ARs is most likely inhibited by the higher coastal mountains on the western edge of the RRW (Figure 3c.), limiting orographic precipitation within the watershed. Future work should calculate the upslope flux of low-level IVT within the RRW to further quantify the results in this paper.

The results from this study highlight the combined importance of the three-dimensional distributions of water vapor flux and its orientation relative to local topography, and the synoptic-scale flow configuration and QG forcing for ascent, on local and regional precipitation extremes associated with landfalling ARs. While this study does not quantify the distinct importance of each ingredient, future work is aimed at (1)

quantifying the impacts of the vertical distribution of water vapor flux and synoptic-scale forcing for ascent on local and regional precipitation distributions during landfalling ARs along the U.S. West Coast and (2) how variability in these quantities influence hydrological extremes that affect both flood control and water supply operations on reservoirs like Lake Mendocino.

References

Baldwin, M. E., and K. E. Mitchell (1997), The NCEP hourly multisensor U.S. precipitation analysis for operations and GCIP research, Preprints, 13th Conf. On hydrology, Am. Meteorol. Soc., pp. 54–55, Long Beach, Calif.

Beebe, R. G., and F. C. Bates (1955), A mechanism for assisting in the release of convective instability, *Mon. Weather Rev.*, *83*(1), 1–10, doi:10.1175/1520-0493(1955)083,0001:AMFAIT.2.0.CO;2.

Bergeron, T. (1965), On the low-level redistribution of atmospheric water caused by orography, *Proc. Int. Conf. On Cloud Physics*, pp. 96–100, IAMAP/WMO, Tokyo, Japan.

Bluestein, H. (1992), *Synoptic–Dynamic Meteorology in Midlatitudes, Principles of Kinematics and Dynamics*, vol I, chap. 5, pp. 282–403, Oxford Univ. Press, Oxford, U. K.

Browning, K. A. and C. W. Pardoe (1973), Structure of low-level jet streams ahead of mid-latitude cold fronts, *Q. J. R. Meteorol. Soc.*, *99*, 619–638, doi:10.1002/qj.49709942204.

Chao, S. (1985), Coastal jets in the lower atmosphere, *J. Phys. Oceanogr.*, *15*, 361–371, doi:10.1175/1520-0485(1985)015<0361:CJITLA>2.0.CO;2.

Cordeira, J. M., F. M. Ralph, and B. J. Moore (2013), The development and evolution of two atmospheric rivers in proximity to western North Pacific tropical cyclones in October 2010, *Mon. Weather Rev.*, *141*, 4234–4255, doi:10.1175/MWR-D-13-00019.1.

Dettinger, M. D., F. M. Ralph, T. Das, P. J. Neiman, and D. Cayan (2011), Atmospheric rivers, floods, and the water resources of California, *Water*, *3*, 455–478, doi:10.3390/w3020445.

Dettinger, M. D. (2013), Atmospheric rivers as drought busters on the U.S. West Coast, *J. Hydrometeorol.*, *14*, 1721–1732, doi:10.1175/JHM-D-13-02.1.

Hartigan, J. A., and M. A. Wong (1979), Algorithm AS 136: A k-means clustering algorithm, *J. R. Stat. Soc.*, *28*(1), 100–108, doi:10.2307/2346830.

Hughes, M., K. M. Mahoney, P. J. Neiman, B. J. Moore, M. Alexander, and F. M. Ralph (2014), The landfall and inland penetration of a flood-producing atmospheric river in Arizona. Part II: Sensitivity of modeled precipitation to terrain height and atmospheric river orientation, *J. Hydrometeorol.*, *15*, 1954–1974, doi:10.1175/JHM-D-13-0176.1.

Keyser, D., B. D. Schmidt, and D. G. Duffy (1992), Quasigeostrophic vertical motions diagnosed from along- and cross-isentrope components of the Q vector, *Mon. Weather Rev.*, *120*, 731–741, doi:10.1175/1520-0493(1992)120<0731:QVMDFA>2.0.CO;2.

Kingsmill, D. E., P. J. Neiman, and A. B. White (2016), Microphysics regime impacts on the relationship between orographic rain and orographic forcing in the coastal mountains of Northern California, *J. Hydrometeorol.*, *17*, 2905–2922, doi:10.1175/JHM-D-16-0103.1.

Lavers, D. A., R. P. Allan, E. F. Wood, G. Villarini, D. J. Brayshaw, and A. J. Wade (2011), Winter floods in Britain are connected to atmospheric rivers, *Geophys. Res. Lett.*, *38*, L23803, doi:10.1029/2011GL049783.

Lavers, D. A., G. Villarini, R. P. Allan, E. F. Wood, and A. J. Wade (2012), The detection of atmospheric rivers in atmospheric reanalyses and their links to British winter floods and the large-scale climatic circulation, *J. Geophys. Res.*, *117*, D20106, doi:10.1029/2012JD018027.

National Weather Service (2015), Product/service description document experimental probabilistic snowfall products. [Available at http://products.weather.gov/PDD/PDD%20for%20Probabilistic%20Snow%20Experiment%202015_2016%20Season.pdf.]

The NCAR Command Language (2017), (version 6.4.0) [software], Boulder, Colorado: UCAR/NCAR/CISL/TDD. [Available at https://doi.org/10.5065/D6WD3XH5.]

Neiman, P. J., F. M. Ralph, A. B. White, D. E. Kingsmill, and P. O. G. Persson (2002), The statistical relationship between upslope flow and rainfall in California's coastal mountains: Observations during CALJET, *Mon. Weather Rev.*, *130*, 1468–1492, doi:10.1175/1520-0493(2002)130.

Neiman, P. J., F. M. Ralph, G. A. Wick, J. D. Lundquist, and M. D. Dettinger (2008), Meteorological characteristics and overland precipitation impacts of atmospheric rivers affecting the West Coast of North America based on eight years of SSM/I satellite observations, *J. Hydrometeorol.*, *9*, 22–47, doi:10.1175/2007JHM855.1.

Neiman, P. J., L. J. Schick, F. M. Ralph, M. Hughes, and G. A. Wick (2011), Flooding in western Washington: The connection to atmospheric rivers, *J. Hydrometeorol.*, *12*, 1337–1358, doi:10.1175/2011JHM1358.1.

Neiman, P. J., F. M. Ralph, B. J. Moore, M. Hughes, K. M. Mahoney, J. M. Cordeira, and M. D. Dettinger (2013), The landfall and inland penetration of a flood-producing atmospheric river in Arizona. Part I: Observed synoptic-scale, orographic, and hydrometeorological characteristics, *J. Hydrometeorol.*, *14*, 460–484, doi:10.1175/JHM-D-12-0101.1.

Ralph, F. M., P. J. Neiman, D. E. Kingsmill, P. O. Persson, A. B. White, E. T. Strem, E. D. Andrews, and R. C. Antweiler (2003), The impact of a prominent rain shadow on flooding in California's Santa Cruz Mountains: A CALJET case study and sensitivity to the ENSO cycle, *J. Hydrometeorol.*, *4*, 1243–1264, doi:10.1175/1525-7541(2003)004<1243:TIOAPR>2.0.CO;2.

Ralph, F. M., P. J. Neiman, and G. A. Wick (2004), Satellite and CALJET aircraft observations of atmospheric rivers over the eastern North Pacific Ocean during the winter of 1997/98, *Mon. Weather Rev.*, *132*(7), 1721–1745, doi:10.1175/1520-0493(2004)132<1721:SACAOO>2.0.CO;2.

Ralph, F. M., P. J. Neiman, G. Wick, S. Gutman, M. Dettinger, D. Cayan, and A. B. White (2006), Flooding on California's Russian River—Role of atmospheric rivers, *Geophys. Res. Lett.*, *33*, L13801, doi:10.1029/2006GL026689.

Ralph, F. M., and M. D. Dettinger (2012), Historical and national perspectives on extreme west coast precipitation associated with atmospheric rivers during December 2010, *Bull. Am. Meteorol. Soc.*, *93*, 783–790, doi:10.1175/BAMS-D-11-00188.1.

Ralph, F. M., P. J. Neiman, R. J. Zamora, and M. D. Dettinger (2013), Observed impacts of duration and seasonality of atmospheric-river landfalls on soil moisture and runoff in coastal in coastal Northern California, *J. Hydrometeorol.*, *14*, 443–459, doi:10.1175/JHM-D-12-076.1.

Ralph, F. M., et al. (2014), A vision for future observations for western U.S. extreme precipitation and flooding, *J. Contemp. Water Res. Education*, *153*, 16–32, doi:10.1111/j.1936-704X.2014.03176.x.

Ralph, F. M., J. M. Cordeira, P. J. Neiman, and M. Hughes, (2016), Landfalling atmospheric rivers, the Sierra barrier jet, and extreme daily precipitation in Northern California's Upper Sacramento River watershed, *J. Hydrometeorol.*, *17*, 1905–1914, doi:10.1175/JHM-D-15-0167.1.

Rutz, J. J., W. J. Steenburgh, and F. M. Ralph (2014), Climatological characteristics of atmospheric rivers and their inland penetration over the western United States, *Mon. Weather Rev.*, *142*(2), 905–921, doi:10.1175/MWR-D-13-00168.1.

Saha, S., et al. (2010), The NCEP Climate Forecast System Reanalysis, *Bull. Am. Meteorol. Soc.*, *91*, 1015–1057, doi:10.1175/2010BAMS3001.1.

Saha, S., et al. (2014), The NCEP Climate Forecast System version 2, *J. Clim.*, *27*, 2185–2208, doi:10.1175/JCLI-D-12-00823.1.

Young, A. M., K. T Skelly, and J. M. Cordeira, 2017, High-impact hydrologic events and atmospheric rivers in California: An investigation using the NCEI storm events database, *Geophys. Res. Lett.*, *44*, 3393–3401, doi:10.1002/2017GL073077.

Zhu, Y., and R. E. Newell (1998), An algorithm for moisture fluxes from atmospheric rivers, *Mon. Weather Rev.*, *126*(3), 725–735, doi:10.1175/1520-0493(1998)126<0725:APAFMF>2.0.CO;2.